Noise Characteristics and Statistics of Picosecond Stokes Pulses Generated in Optical Fibers Through Stimulated Raman Scattering

Clifford Headley, III, and Govind P. Agrawal, *Senior Member, IEEE*

Abstract— **The growth of the Stokes pulse from spontaneous noise during stimulated Raman scattering of picosecond pump pulses in optical fibers, is investigated by using a Langevin-noise term in the coupled nonlinear Schrödinger equations, which include pump depletion, group-velocity mismatch, fiber dispersion, and self- and cross-phase modulation. The model makes use of the actual Raman-gain spectrum of optical fibers. Numerical simulations are used to examine the average behavior of the Stokes pulse, and shot-to-shot fluctuations that are likely to occur in practice. It is shown that the Raman-induced energy transfer is significantly affected by group-velocity dispersion for pump-pulse widths shorter than 5 ps. Examination of the average temporal width shows that the Stokes pulse is initially as wide as the pump pulse, undergoes a gain induced compression and then rebroadens for distances longer than a walk-off length. The effect of varying pump and fiber parameters is to change the minimum value of the Stokes-pulse width, and the distance at which the minimum occurs. The shot-to-shot energy and pulse-width fluctuations initially increase before being reduced at fiber lengths longer than the walk-off length. The primary effect of dispersive and nonlinear effects is to change the distance beyond which fluctuations decrease.**

I. Introduction

ADVANCES IN fiber-optic communications require an understanding of the nonlinear effects which take place as ultrafast pulses propagate in an optical fiber [1]. These nonlinearities arise because fibers confine an intense pulse within a small area over a long distance. One important nonlinear effect is stimulated Raman scattering (SRS) [1]–[5]. This is a process by which a fraction of the power from an optical field (the pump field) incident on an optical fiber is converted into an emitted field (the Stokes field), whose frequency is red-shifted away from the frequency of the incident beam. This process can be initiated by 1) spontaneously scattered photons which are subsequently amplified as they propagate with the pump beam, 2) propagating a weak optical pulse whose frequency difference with an intense copropagating pump pulse falls within the Raman-gain bandwidth, or 3) high-frequency components of a single pulse pumping lower frequency components of the same pulse. The first case describes Raman generation [6], the second Raman amplification [7], and the final intrapulse stimulated Raman scattering [8], [9]. Additional nonlinear effects in optical fibers include self-phase modulation (SPM) [10] and cross-phase modulation (XPM) [11]. These nonlinearities arise from the intensity dependence of the refractive index. SPM refers to the self-induced phase shift experienced by a pulse, and XPM refers to the phase shift induced on one pulse by another copropagating pulse which may be at a different wavelength.

The study of SRS in fibers is of interest both for its detrimental and beneficial effects. For high intensities and long transmission lengths SRS can introduce a power-dependent loss mechanism, as well as crosstalk in multichannel communication systems. On the other hand, SRS in optical fibers can be used for making broadband amplifiers, wavelength-tunable lasers, and pulse compressors.

One problem in the study of SRS is how to model the noise that is an inherent part of the process. During Raman generation, the Stokes pulse builds up from noise, while noise is added to the signal pulse during Raman amplification. Past methods for including spontaneous Raman scattering have relied on the insertion of a weak Stokes signal at the fiber input or inserted a constant source along the fiber [12]–[14] While this method allows the study of the effects of walk-off, SPM and XPM, the shape and width of the input seed pulse influences the output characteristics of the Stokes pulse.

The effect of noise during SRS has been studied extensively in gases [15]–[19]. However, there are important differences between gases and fibers. The shape and the width of the Raman-gain spectrum in fibers is quite different from that of gases [3]–[5]. The Raman-gain spectrum of gases can be modeled with a Lorentzian lineshape, while there are no good analytic expressions for the gain curve of fibers. In addition, the gain curve of optical fibers is extremely broad ($\approx$8 THz) compared to gases (640 MHz at 15 atm in H_2) [20]. Furthermore, group-velocity dispersion (GVD) which is negligible in gases becomes important for pulse propagation in optical fibers. Finally, nonlinear effects such as SPM and XPM, which have not been addressed in the study of gases must be considered in optical fibers.

In this paper, a realistic model is presented that effectively simulates the actual noise process that leads to the growth of the Stokes pulse during SRS. In addition the Raman-gain spectrum obtained from experimental data is used in the numerical simulations [21]. The results of numerical simulations showing

Manuscript received November 29, 1994; revised June 27, 1995. This work supported in part by the U.S. Army Research Office.

C. Headley, III was with the Institute of Optics, University of Rochester, Rochester, NY 14627 USA. He is now with AT&T Bell Laoratories, 600 Mountain Avenue, Room 6D225, Murray Hill, NJ 07974 USA.

G. P. Agrawal is with the Institute of Optics, University of Rochester, Rochester, NY 14627 USA.

IEEE Log Number 9414618.

the dynamics of the Stokes pulse formation and its statistical properties are then studied. This paper is organized as follows. In Section II coupled nonlinear Schrödinger equations which include a Langevin noise term to represent spontaneous noise in the fiber are derived. The appropriate value of the noise term is calculated in Section III, and in Section IV numerical implementation of the model is discussed. In Section V, the behavior of the Stokes pulse in the time and frequency domains is studied for a given set of parameters. The effect of varying these parameters on the average Stokes pulse energy and rms width is explored in Section VI. Section VII examines statistics of shot-to-shot fluctuations for various pump pulse and fiber values. The results are summarized in Section VIII.

II. Theoretical Model

When an optical pulse propagates in a fiber, it affects the polarizability of the silica molecules in two ways. The electronic structure is altered on what is essentially an instantaneous time scale, leading to an intensity-dependent refractive index. In addition, this perturbation in electronic structure leads to a change in the field seen by the nuclei of the molecule, and may result in the vibration of the molecule. This molecular vibration is an intrinsic part of the Raman effect. In addition to these two contributions, vibration of the molecule can occur spontaneously through, for example, thermal noise. A third-order nonlinear polarization, $\boldsymbol{P}_{NL}(\boldsymbol{r},t)$, which accounts for these three effects can be written as the sum of the instantaneous electronic or Kerr polarization $\boldsymbol{P}_K(\boldsymbol{r},t)$, a Raman polarization $\boldsymbol{P}_R(\boldsymbol{r},t)$, and a noise polarization $\boldsymbol{P}_N(\boldsymbol{r},t)$ as [22]–[25]

$$\begin{aligned}\boldsymbol{P}_{NL}(\boldsymbol{r},t) &= \boldsymbol{P}_K(\boldsymbol{r},t)+\boldsymbol{P}_R(\boldsymbol{r},t)+\boldsymbol{P}_N(\boldsymbol{r},t)\\ &= \varepsilon_0\boldsymbol{E}(\boldsymbol{r},t)\Big\{\chi_K\boldsymbol{E}(\boldsymbol{r},t)\cdot\boldsymbol{E}(\boldsymbol{r},t)\\ &\quad+\int_{-\infty}^{\infty}\chi_R(t-t')\boldsymbol{E}(\boldsymbol{r},t')\cdot\boldsymbol{E}(\boldsymbol{r},t')\,dt'\\ &\quad+\int_{-\infty}^{\infty}\chi_N(t-t')F_N(t')\,dt'\Big\},\end{aligned}\tag{1}$$

where $\boldsymbol{E}_{r,t}$ is the electric field, ε_0 is the permittivity of free space, χ_K is the Kerr susceptibility representing the contributions of electrons to the nonlinear process, $\chi_R(t)$ is a third-order time-dependent nonlinear susceptibility which accounts for Raman scattering, $F_N(t)$ is a Langevin noise force representing all the processes, which lead to random vibrations of silica molecules, and $\chi_N(t)$ is the response function that converts $F_N(t)$ into a spontaneous polarization. $\chi_R(t)$ and $\chi_N(t)$ were obtained using a simple harmonic oscillator equation to describe the displacement of a molecule [25]–[27]. The driving forces for the oscillator were the applied field and a randomly varying force that simulated noise. The form of this equation is similar to a Langevin equation hence the use of the term Langevin noise force. This equation can be solved in the frequency domain, and its solution has two terms, one containing the applied electric field, and the other the random noise force. The displacement can be related to the polarization with the first term leading to the Raman polarization, and the second term leading to the noise polarization. Explicit expressions for $\chi_R(t)$ and $\chi_N(t)$ can be obtained by following this procedure [25]–[27]. Unfortunately, due to the amorphous nature of silica fibers, wherein many closely spaced vibrational levels contribute to the scattering process it is difficult to calculate the values of these parameters [25]. It should also be noted that the form of the second term on the right-hand side of (1) suggests that $\chi_R(t)$ is the Raman response function presented in several recent articles [22], [23].

Coupled nonlinear Schrödinger equations which include the first term in (1) are well known [1], [14], hence the focus here is how to incorporate the Raman and noise polarizations into coupled nonlinear Schrödinger equations. To proceed, the Fourier transform of the last two terms in (1) can be written as [22]–[24]

$$\begin{aligned}\tilde{P}_R(\boldsymbol{r},\omega) &= \varepsilon_0\int_{-\infty}^{\infty}\int_{-\infty}^{\infty}\tilde{\chi}_R(\omega_1-\omega_2)\tilde{E}(\boldsymbol{r},\omega_1)\tilde{E}(\boldsymbol{r},\omega_2)\\ &\quad\cdot\tilde{E}(\boldsymbol{r},\omega-\omega_1+\omega_2)\,d\omega_1\,d\omega_2,\end{aligned}\tag{2}$$

and

$$\tilde{P}_N(\boldsymbol{r},\omega) = \varepsilon_0\int_{-\infty}^{\infty}\tilde{\chi}_N(\omega-\omega_1)\tilde{F}_N(\omega-\omega_1)\tilde{E}(\boldsymbol{r},\omega_1)\,d\omega_1,\tag{3}$$

Both $\boldsymbol{E}$ and $\boldsymbol{P}$ are assumed to be linearly polarized, and a tilde denotes the Fourier transform. If we assume the anti-Stokes components do not grow significantly, the electric field can be written as the sum of the pump and Stokes waves in the form

$$\begin{aligned}E(\boldsymbol{r},t) &= \tfrac{1}{2}\{A_p(z,t)e^{i(\beta_p z-\omega_p t)}\\ &\quad+A_s(z,t)e^{i(\beta_s z-\omega_s t)}\}T(x,y)+\text{ c.c.}\end{aligned}\tag{4}$$

Here $A_j(z,t)$ with $j=p$ or s is the (complex) amplitude of the pump and Stokes pulse envelopes respectively, ω_j is the carrier frequency, β_j is the mode propagation constant, and $T(x,y)$ is the distribution of the field perpendicular to the direction of propagation and is assumed to be equal for both waves. The use of a carrier frequency is for convenience and does not mean that the spectral width of the Stokes pulse is narrow. The noise force can also be expressed in phasor form as,

$$F_N(\boldsymbol{r},t) = \tfrac{1}{2}\{f_N(z,t)e^{i(\beta_R z-\Omega_R t)}+f_N^*(z,t)e^{-i(\beta_R z-\Omega_R t)}\}\tag{5}$$

where $f_N(z,t)$ is a slowly and randomly varying function of the noise, $\Omega_R=\omega_p-\omega_s$ is the difference between the carrier frequencies of the pump and Stokes waves, $\beta_R=\beta_p-\beta_s$ is the difference between propagation constants of the pump and Stokes waves, and f_N is taken as a Gaussian white noise with the statistical properties [15], [16]

$$\begin{aligned}\langle f_N(z,t)\rangle &= 0,\\ \langle f_N(z,t)f_N^*(z',t')\rangle &= 2D\delta(z-z')\delta(t-t').\\ \langle f_N(z,t)f_N(z',t')\rangle &= \langle f_N^*(z,t)f_N^*(z',t')\rangle = 0.\end{aligned}\tag{6}$$

The symbol $\langle\cdots\rangle$ indicates an ensemble average, and D is a diffusion constant, the value of which will be determined later.

Substituting the Fourier transform of (4) into (2) and carrying out the indicated multiplications yields 64 terms, of which only 36 terms are phase-matched. Among the 36 phase-matched terms, 28 of the terms are approximately zero [24] due to the finite extent of both the Raman gain curve and the spectrum of the pump and Stokes waves. The inverse Fourier transform of the remaining 8 terms yields the following expression for the contribution of the pump and Stokes wave to the Raman polarization $P_{Rp}(r,t)$ and $P_{Rs}(r,t)$, respectively

$$P_{Rp}(r,t) = \tfrac{1}{4}\varepsilon_0 T^3(x,y) A_p(z,t) A_s(z,t) \cdot \left[\int_{-\infty}^{\infty} \tilde{\chi}_R(\omega' + \Omega_R)\tilde{A}_s^*(-\omega') e^{-i\omega' t}\, d\omega'\right] \cdot e^{i(\beta_p z - \omega_p t)} \tag{7}$$

and

$$P_{Rs}(r,t) = \tfrac{1}{4}\varepsilon_0 T^3(x,y) |A_p(z,t)|^2 \cdot \left[\int_{-\infty}^{\infty} \tilde{\chi}_R(\omega' - \Omega_R)\tilde{A}_s(\omega') e^{-i\omega' t}\, d\omega'\right] \cdot e^{i(\beta_s z - \omega_s t)}. \tag{8}$$

Equations (7) and (8) assume that the pump spectrum is very narrow compared to the Raman gain spectrum, which is true for pulse widths greater than 1 ps. A similar expression can be obtained for the noise portion of the polarization by substituting (4) and (5) into (3) yielding for the pump and Stokes noise contributions $P_{Np}(r,t)$ and $P_{Ns}(r,t)$, respectively,

$$P_{Np}(r,t) = \tfrac{1}{4}\varepsilon_0 T(x,y) A_s(z,t) \cdot \left[\int_{-\infty}^{\infty} \tilde{\chi}_N(\omega' + \Omega_R)\tilde{f}_N(\omega') e^{-i\omega' t}\, d\omega'\right] \cdot e^{i(\beta_p z - \omega_p t)}, \tag{9}$$

and

$$P_{Ns}(r,t) = \tfrac{1}{4}\varepsilon_0 T(x,y) A_p(z,t) \cdot \left[\int_{-\infty}^{\infty} \tilde{\chi}_N(\omega' - \Omega_R)\tilde{f}_N^*(-\omega') e^{-i\omega' t}\, d\omega'\right] \cdot e^{i(\beta_s z - \omega_s t)}. \tag{10}$$

To incorporate (7)–(10) into coupled amplitude equations for the pump and Stokes wave, the starting point is Maxwell's wave equation

$$\nabla^2 \boldsymbol{E}(\boldsymbol{r},t) - \frac{1}{c^2}\frac{\partial^2 \boldsymbol{E}(\boldsymbol{r},t)}{\partial t^2} = \mu_0 \frac{\partial^2 \boldsymbol{P}_L(\boldsymbol{r},t)}{\partial t^2} + \mu_0 \frac{\partial^2 \boldsymbol{P}_{NL}(\boldsymbol{r},t)}{\partial t^2} \tag{11}$$

where $\boldsymbol{P}_L(\boldsymbol{r},t)$ is the linear contribution to polarization, c is the velocity of light in vacuum, and μ_0 is the vacuum permeability. By substituting (4), and (7)–(10), into (1), placing the result along with (4) into (11), using the expression for $\boldsymbol{P}_L(\boldsymbol{r},t)$ in [1], and assuming 1) the pump and Stokes pulses maintain their polarization along the fiber, 2) the nonlinear and noise contributions to $\boldsymbol{P}_{NL}(\boldsymbol{r},t)$ are a small perturbation to the refractive index, and 3) the loss in the fiber can be neglected, and following the derivation laid out in [1] the following coupled equations for the pump and Stokes waves are obtained:

$$\frac{\partial u_p}{\partial z} + \frac{1}{v_{gp}}\frac{\partial u_p}{\partial t} + i\frac{\beta_{2p}}{2}\frac{\partial^2 u_p}{\partial t^2} = i\gamma_p u_p[|u_p|^2 + 2(1-\delta)|u_s|^2] + \frac{i}{2}u_p u_s \int_{-\infty}^{\infty} \tilde{G}_p(\omega' + \Omega_R)\tilde{u}_s^*(-\omega') e^{-i\omega' t}\, d\omega' + \frac{i}{2}u_s \int_{-\infty}^{\infty} \tilde{H}_p(\omega' + \Omega_R)\tilde{f}_N(z,\omega') e^{-i\omega' t}\, d\omega' \tag{12}$$

and

$$\frac{\partial u_s}{\partial z} + \frac{1}{v_{gs}}\frac{\partial u_s}{\partial t} + i\frac{\beta_{2s}}{2}\frac{\partial^2 u_s}{\partial t^2} = i\gamma_s u_s[|u_s|^2 + 2(1-\delta)|u_p|^2] + \frac{i}{2}|u_p|^2 \int_{-\infty}^{\infty} \tilde{G}_s(\omega' - \Omega_R)\tilde{u}_s(\omega') e^{-i\omega' t}\, d\omega' + \frac{i}{2}u_p \int_{-\infty}^{\infty} \tilde{H}_s(\omega' - \Omega_R)\tilde{f}_N^*(z,-\omega') e^{-i\omega' t}\, d\omega'. \tag{13}$$

In (12) and (13), β_{2j} is the GVD coefficient, δ is the fraction of the XPM contribution which arises from molecular vibrations [22], [24], and v_{gj} is the group velocity. The lack of symmetry in (12) and (13) is due to the assumption that the pump pulse spectral width is much narrower than the spectral width of the Raman gain curve. The variables $u_j(z,t), \tilde{G}_j(\omega), \gamma_j$, and $\tilde{H}_j(\omega)$ are defined as follows:

$$u_j = \kappa A_j \left(\int_{-\infty}^{\infty} T^2(x,y)\, dx\, dy\right)^{1/2} \quad \tilde{G}_j(\omega) = \frac{k_j \tilde{\chi}_R(\omega)}{2n\kappa^2 A_{\text{eff}}}$$
$$\gamma_j = \frac{k_j n_2}{A_{\text{eff}}\kappa^2} \quad \tilde{H}_j(\omega) = \frac{k_j \tilde{\chi}_N(\omega)}{2n} \tag{14}$$

where κ is introduced to normalize u_j such that $|u_p|^2$ represents power. κ and A_{eff} are defined as

$$\kappa^2 = \frac{1}{2}n\left(\frac{\varepsilon_0}{\mu_0}\right)^{1/2} \quad A_{\text{eff}} = \frac{\left(\iint T^2\, dx\, dy\right)^2}{\iint T^4\, dx\, dy} \tag{15}$$

and $k_j = 2\pi/\lambda_j$ is the vacuum wavenumber, n is the linear refractive index, $n_2 = 3\mathrm{X}_K/8n$ is the nonlinear coefficient, and A_{eff} is the effective core area of the fiber. The first terms on the right-hand side of (12) and (13) account for SPM and XPM, the real part of the third term is an additional contribution to XPM, while the imaginary part is responsible for the Raman gain, and finally the fourth term accounts for linearly amplified noise in the system.

III. Physical Parameters

The relationship between $\tilde{G}_j(\omega)$ in (12) and (13) and the gain and index spectra associated with SRS are well known [22]–[25]. The imaginary part of $\tilde{G}_j(\omega)$ is equal to the Raman gain $g_j(\omega)$, and the real part of $\tilde{G}_j(\omega)$ can be calculated from

$g_j(\omega)$ using the Kramers-Kronig relationship. Less well known is the relationship between $\tilde{H}_j(\omega)$ and physical parameters.

In order to calculate the value of $\tilde{H}_j(\omega)$, the spectral density of the Stokes pulse must be calculated in the linear regime, where spontaneous scattering is the most important term in the Stokes equation. Assuming i) the length of fiber under consideration is short enough that dispersion and pump depletion effects are negligible, ii) the pump power is small enough that nonlinear effects can be neglected, and iii) the pump pulse temporal width is broad enough that its spectrum is a delta function compared to the noise and Raman gain spectrum, (13) reduces to

$$\frac{\partial u_s(z,t)}{\partial z} = \frac{i}{2}u_p \int_{-\infty}^{\infty} \tilde{H}_s(\omega' - \Omega_R)\tilde{f}_N^*(z,-\omega')e^{-i\omega' t}\, d\omega'. \tag{16}$$

Taking the Fourier transform of (16) and integrating over z yields,

$$\tilde{u}_s(L,\omega) = \frac{i}{2}u_p\tilde{H}_s(\omega - \Omega_R)\int_0^L \tilde{f}_N^*(z',-\omega)\, dz' \tag{17}$$

where L is the length of fiber under consideration. The spectral density, $S(\omega)$, is defined as [28]

$$S(\omega) = \lim_{T\to\infty}\left\langle \frac{1}{T}|\tilde{u}_s(L,\omega)|^2 \right\rangle \tag{18}$$

where $u_s(L,t) = 0$ when $t > T$. Substituting (17) into (18) and carrying out the ensemble average indicated using (6), the spectral density is given by

$$S(\omega) = D|u_p|^2|\tilde{H}_s(\omega - \Omega_R)|^2 L. \tag{19}$$

$S(\omega)$ can now be related to the Raman-scattering cross section $\sigma_s(\omega)$, which is defined as the fraction of pump photons incident on a medium that is scattered per unit distance, per unit solid angle, per unit frequency and is given in SI units by [12], [13],

$$\sigma_s(\omega) = \frac{chn^2}{\lambda_s^3}g_s(\omega)[\eta(\omega) + 1] \tag{20}$$

where h is the Planck constant, $\eta = [\exp(h\omega/k_BT) - 1]^{-1}$ is the Bose-Einstien population factor, k_B is the Boltzmann constant, and T the temperature of the fiber. Equation (19) can be cast into the form of (20) by dividing it by the pump power, fiber length and solid angle. Equating this result to $\sigma_s(\omega)$ yields,

$$D|\tilde{H}_s(\omega - \Omega_R)|^2 = f\pi(\text{N.A.})^2\sigma_s(\omega) \tag{21}$$

where f is the fraction of light scattered per steradian that is guided, and N.A. is the numerical aperture of the fiber [12], [13]. Assuming $\tilde{H}_s(\omega)$ is real, this means the form and amplitude of the parameters needed to calculate the numerical values of the noise terms in (12) and (13) are known. The result given in (21) agrees with the value of the input seed Stokes pulse used in some previous work, the difference here is that the noise source is now being treated as a random variable [13].

IV. Computer Model

Equations (12) and (13) are the propagation equations for the study of Stokes pulse formation. A numerical code was written based on the fast-Fourier-transform (FFT) split-step method to simulate evolution of the pump and Stokes pulses [1]. The Raman gain spectrum used for these simulations was obtained from measured data [21]. The noise force, $f_N(z,t)$ is simulated by random numbers generated with a Gaussian distribution of zero mean and unit variance [29]. The complex amplitude, $u_j(z,t) = |u_j(z,t)|\ \exp[i\phi(z,t)]$, of the pump and Stokes pulses after propagating a distance z is used to obtain the pulse shape governed by the intensity profile $|u_j(z,t)|^2$. The pulse spectrum $|\tilde{u}_j(z,\nu)|^2$ is obtained by taking the Fourier transform of $u_j(z,t)$. The parameter used to quantify the temporal pulse widths the rms width $\tau(z)$ which is defined as

$$\tau^2(z) = \frac{\displaystyle\int_{-\infty}^{\infty} t^2|u_s(z,t)|^2\, dt - \left(\int_{-\infty}^{\infty} t|u_s(z,t)|^2\, dt\right)^2}{\displaystyle\int_{-\infty}^{\infty}|u_s(z,t)|^2\, dt}. \tag{22}$$

The shot-to-shot fluctuations that would be observed in the laboratory were obtained by repeating the simulation of the passage of the pump and Stokes pulses many times through the fiber. For each trail, the value of $f_N(z,t)$ was fluctuating leading to quantifiable differences in the Stokes pulse energy and rms width. In this way ensembles of these parameters under various conditions were collected.

Several tests were applied to the code. Simulations with the input parameters used to obtain the results given in [1, ch. 8], with the noise term set to zero were performed, and the results agreed with the previously published results. In order to test the noise term, simulations were performed to produce the experimental results given in [6].

The simulations correspond to the experimental situation of a Nd:YAG laser source producing Gaussian-shaped picosecond pulses at 1.064 μm, coupled into a single-mode optical fiber, and producing Stokes pulses at 1.12 μm. The fiber parameters are taken from [6] and are $\beta_{2p} = 25.2$ ps ^{2} km^{-1}, $\gamma_p = 5.06$ km^{-1} W^{-1} and $g_p = 2.34$ km^{-1} W^{-1}. The value of these parameters for the Stokes pulse is calculated by multiplying them by the ratio $\lambda_p/\lambda_s = 0.95$. The walk-off between the two pulses is governed by the parameter d, defined as

$$d = \frac{1}{v_{gp}} - \frac{1}{v_{gs}} \tag{23}$$

and was set to $d = 2.2$ ps/m. Furthermore $\delta = 0.2$ and $f = 0.5$ are used in (21) [12], [13].

In order to quantify the relative importance of various parameters, two length scales are used [1],

$$L_D = \frac{T_0^2}{|\beta_{2p}|}, \quad \text{and} \quad L_w = \frac{T_p}{|d|}. \tag{24}$$

The dispersion length and the effective walk-off length describe respectively the length scales over which GVD and

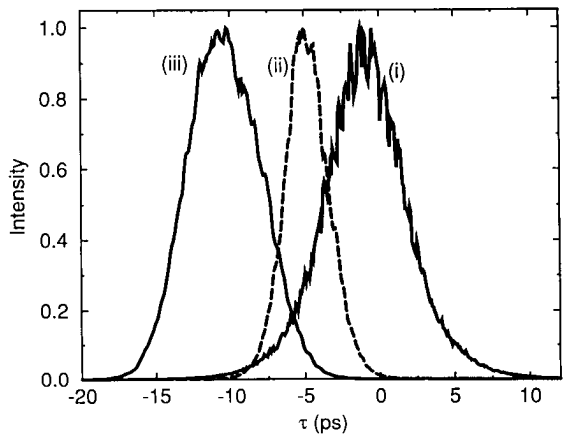

Fig. 1. Normalized Stokes pulse intensity profiles at (i) 0.25 L_w, (ii) L_w, and (iii) 2 L_w. T_p = 10 ps and the input pump power is 1.2 $P_{\rm th}$. Fiber parameters are β_{2p} = 25.2 ps^2 km^{-1}, γ_s = 5.06 km^{-1} W^{-1}, g_p = 2.34 km^{-1} W^{-1}, β_{2s} = 23.8 ps^2 km^{-1}, γ_s = 4.79 km^{-1} W^{-1}, g_s = 2.21 km^{-1} W^{-1}, and d = 2.2 ps/m.

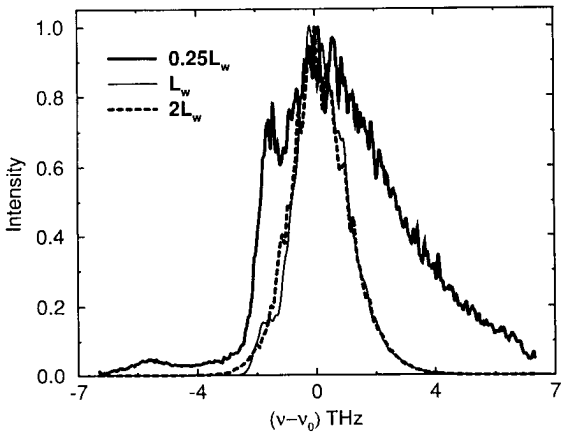

Fig. 2. Normalized Stokes pulse spectrum profiles at 0.25 L_w (dark solid line), L_w (solid line) and 2 L_w (dashed line). The pulse and fiber parameters are identical to Fig. 1.

walk-off become important. T_0 is the 1/e-intensity pulse width and T_p is the intensity full width at half-maximum of the pump pulse. For Gaussian pulses, the two are related through the expression T_p = 1.665 T_0. For a T_p = 10-ps pulse, L_D = 1.4 km and L_w = 4.5 m. The walk-off length can be used to calculate a threshold power, $P_{\rm th}$, from the criterion [1],

$$G_A = g_p P_{\rm th} L_w = 16. \tag{25}$$

This yields a threshold power of approximately 1500 W. The results of simulations are presented in the following sections for different peak pump powers temporal widths and various fiber parameters.

V. Averaged Pulse Shapes and Spectra

Fig. 1 shows Stokes pulse shapes, averaged over 300 shots, at fiber lengths of (i) $0.25L_W$, (ii) L_W, and (iii) $2L_W$, for an input pump-pulse power of P_0 = 1.2 $P_{\rm th}$ and T_p = 10 ps. The pulse shapes have all been normalized with respect to their individual peak power values.

Fig. 1 shows that the temporal width of the Stokes pulse initially narrows, and then widens. This behavior can be explained as follows. The amplification of the Stokes pulse by the pump pulse is proportional to the factor $\exp(g_p|u_p(z,t)|^2 z)$. Due to the time dependence of the pump power, the gain experienced by the Stokes pulse will vary across its temporal profile. Initially the center portion of the Stokes pulse, which overlaps with the center of the pump pulse, experiences more amplification than the wings causing gain narrowing of the pulse width. As the Stokes pulse walks away from the pump pulse, the center of the pump pulse amplifies the trailing edge of the Stokes pulse increasing the Stokes pulse temporal width. In Fig. 1 it is seen that at z = 2 L_W the Stokes pulse has developed a tail on the right side. This feature is easily understood by noting that in the case of normal GVD the trailing edge of the Stokes pulse continues to overlap with the pump pulse and is continuously being amplified, while the leading edge has completely walked out of the pump pulse. Note also that the high-frequency oscillations seen at z = 0.25 L_w [curve (i)] decrease as the Stokes pulse propagates along the fiber. Initially the Stokes pulse is formed out of noise, and a noisy structure shows up in the Stokes intensity profile. As the process becomes stimulated, the high-frequency oscillations dampen out.

Fig. 2 shows the Stokes-pulse spectra that correspond to the pulse shapes shown in Fig. 1. The Stokes-pulse spectrum narrows as the pulse propagates through the fiber because of gain narrowing as discussed above. This compression can be accounted for by considering the spectral shape of the Raman gain curve, which peaks at the center frequency of the Stokes light. The center frequencies of the Stokes spectrum are preferentially amplified over the wings, and narrowing of the spectrum occurs. For the parameters used, the effects of SPM and XPM are negligible.

VI. Evolution of Average Stokes Pulse Energy and Width

In order to compare the effect of different pump pulse and fiber parameters on the average Stokes pulse characteristics, it is useful to introduce the following normalized quantities. The energy growth factor G is defined as

$$G(z) = \frac{\int_{-\infty}^{\infty} |u_s(z,t)|^2\, dt}{\int_{-\infty}^{\infty} |u_p(0,t)|^2\, dt} \tag{26}$$

while the normalized propagation distance ξ, and the normalized Stokes rms width X are defined respectively as

$$\xi = \frac{z}{L_w} \quad \text{and} \quad X(\xi) = \frac{\tau_s(\xi)}{\tau_p(0)}. \tag{27}$$

Fig. 3 shows the variation of the energy amplification factor $G(\xi)$ in decibels as a function of the normalized distance ξ. An important point to be made is that the values of $P_{\rm th}$ and L_w change for the different conditions described and whenever appropriate, these values were recalculated. The simulations show that the energy in the Stokes pulse steadily increases due to SRS, with the rate of energy increase eventually

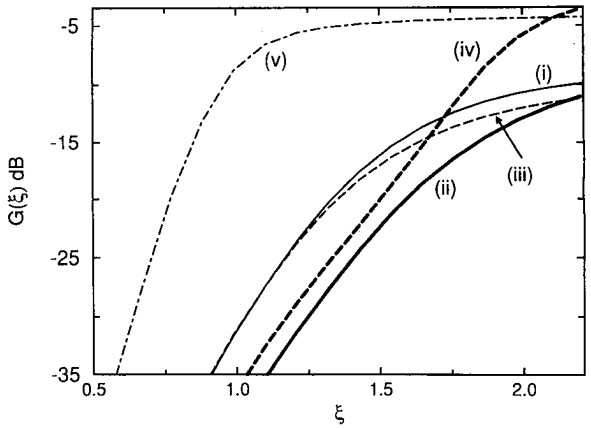

Fig. 3. Average Stokes pulse energy normalized to input pump energy and expressed in decibels versus distance expressed as a fraction of the walk-off length, (i) for the same parameters as Fig. 1 with the other curves having the following exceptions, (ii) $T_p = 2$ ps, (iii) $T_p = 10$ ps and $\beta_{2p} = \beta_{2s} = 0$, (iv) $T_p = 2$ ps and $\beta_{2p} = \beta_{2s} = 0$, and (v) $T_p = 10$ ps and input pump power equal 1.5 P_{th}.

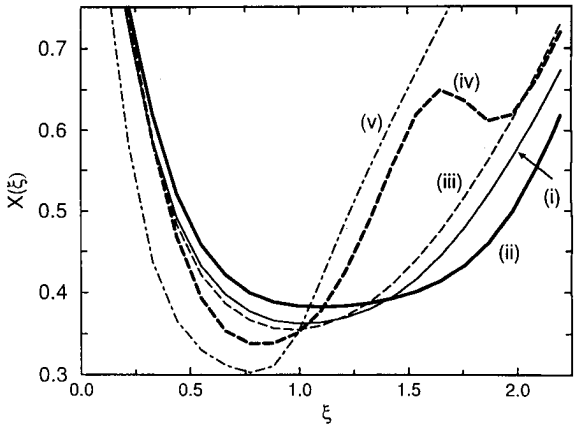

Fig. 4. Average Stokes pulse rms width normalized with respect to the input pump pulse rms width, versus distance expressed as a fraction of the walk-off length, with parameters corresponding to those in Fig. 3 for the various curves.

approaching zero due to the walk-off between the Stokes and pump pulses. Curve (i) in Fig. 3 is obtained under the same conditions as in Fig. 1.

The result of reducing the input pump pulse width from 10 ps to 2 ps is shown by curve (ii) in Fig. 3. The initial amplification of the Stokes pulse is reduced compared with the case of a 10-ps pump pulse. However, by 2 L_w the energy transfered to the Stokes pulse for the two pulse widths are approximately equal. This behavior can be understood as follows. Equations (24) show that the effect of dispersion is greater for a 2-ps pump pulse than for a 10-ps pump pulse, as a result the 2-ps pump pulse will broaden faster than the 10-ps pump pulse. This broadening means that the intensity of the pump pulse is reduced and less amplification takes place for the 2-ps pump pulse. However, because of the increased spreading of the pump pulse due to GVD, the Stokes pulse continues to overlap with the pump pulse for a longer length of fiber, so that at $\xi = 2$, the amplification factor for the two cases are about equal.

The effect on the energy growth of the Stokes pulse of neglecting GVD for input pump pulse widths of 10 ps and 2 ps is shown by curves (iii) and (iv), respectively. The results are quite different for the two cases. This is because the effect of GVD on the amplification process is both beneficial and detrimental. It is beneficial to amplification because during walk-off the Stokes wave will interact with the pump pulse over a longer length of fiber due to dispersion-induced broadening of the pump pulse. The dispersion is detrimental to amplification because as the pump pulse broadens, the intensity of the pump profile is reduced so that the amplification of the Stokes pulse decreases. When the dispersion length is long, and the effect of dispersion is small, dispersion benefits the amplification process which is the case for 10-ps pulses. When the dispersion length is short, the detrimental aspect of dispersion is more important which is the case for 2-ps pulses. These results are reflected in the curves of Fig. 3, and are similar to that obtained by Scalora *et al.* [19] if we note that GVD is the temporal analog of diffraction.

Finally, the effect of increasing the pump power is shown by curve (v) of Fig. 3. There is an increase in energy transfered to the Stokes pulse, a consequence of gain being proportional to the exponential of the pump pulse.

Fig. 4 is a plot of the normalized rms Stokes width X as a function of ξ. The five curves shown correspond to the same conditions as in Fig. 3. Curve (i) is for conditions identical to that in Fig. 1 and shows the narrowing and eventual broadening of the Stokes pulse. The effect of decreasing input-pump pulse width is shown by curve (ii) in Fig. 4. The narrowing of the Stokes pulse is reduced, but the pulse remains at its minimum width for a longer length of fiber. Both of these results can be explained by considering the increased GVD-induced broadening of the pump pulse resulting from the reduction of its input pulse width. As a result of greater pulse broadening, the difference between the amplification factors at the center and wings of the Stokes pulse (as it walks off from the pump pulse) is reduced, leading to less gain narrowing of the Stokes pulse. In addition the increased flattening of the pump pulse means that once the Stokes pulse has reached its minimum width it remains narrow for a longer distance, because the center of the pulse is amplified at nearly the same rate as the wings.

The effect of neglecting dispersion for 10-ps [curve (iii)] and 2-ps [curve (iv)] pump pulses respectively on the Stokes pulse rms width is shown in Fig. 4. In both cases the pulse narrowing has increased and broadening occurs at a shorter fiber length than without GVD. In the absence of GVD, the pulse shape remains unchanged. The decrease in the rms width of the Stokes pulse is due to the lack of GVD-induced broadening of the pump pulse. The difference between the amplification factor of the center and wings of the Stokes pulse is larger without GVD, leading to more gain narrowing. The increase in the eventual broadening of the Stokes pulse over the situation where there is GVD is a continuation of this argument. The center of the pump pulse is not decreasing in intensity as the Stokes pulse walks off, so therefore it is able to more quickly amplify the wings of the Stokes pulse, leading to the increased broadening seen in Fig. 4. For the case of a 2-ps pump pulse two minima are observed. This is because the intensity of the

pump pulse remains large enough that a second Stokes pulse builds up after the major portion of the first Stokes pulse has walked away from the pump pulse.

Finally, curve (v) in Fig. 4 shows that the effect of increasing the pump power is to cause a decrease in the minimum rms pulse width of the Stokes pulse, over a shorter length of fiber. However, broadening of the Stokes pulse occurs at a much faster rate. The explanation for this runs parallel to that given above when GVD is neglected. An increased pump power, increases the difference in amplification factors between the center and wings of the Stokes pulse, thereby increasing the gain narrowing experienced. This increased pump power also means that the wings of the Stokes pulse are more strongly amplified during walk-off, leading to an increased broadening of the Stokes pulse over a shorter distance.

VII. Statistics of Fluctuations

Fluctuations in the Stokes-pulse energy and temporal shape arise because of the uncertainty in the time, position and energy of the first few spontaneously scattered photons, that will be amplified to produce the Stokes light. This leads to variations in the macroscopic properties of the Stokes pulse. In the following subsections the statistics of the energy and the rms width of the Stokes pulse are investigated. The work is also compared to that done with gases [15]–[19].

In the work done on gases several criteria were used to chart the behavior of Raman statistics. One criterion for determining when the Stokes pulse energy and width statistical distributions changed from exponential to Gaussian is given by [15]–[17]: $\Gamma T_p > 2g_p|u_p(0,t)|^2 z$, where Γ is the full width at half maximum of the Raman gain spectrum. A value of $\Gamma = 8$ THz will be used for the discussions to follow. This criterion can be expressed in terms of a variable m as

$$m = \frac{\Gamma T_p}{2g_p|u_p(0,t)|^2 z}. \tag{28}$$

The transition from exponential to Gaussian statistics is of interest because in the work done on gases this change marked the change in Stokes amplification from the linear (undepleted pump) region to the nonlinear (depleted pump) region.

A. Pulse Energy

Fig. 5 is the energy distribution function for the Stokes pulse, for a sample of 300 shots, at walk-off lengths of 0.015 L_w, L_w, and 2.5 L_w. The pulse and fiber parameters are the same as in Fig. 1. In Fig. 5, the curve at a distance of 0.015 L_w shows that the Stokes energy distribution is nearly Gaussian. As the pulse propagates further along the fiber it loses its Gaussian like shape. Not only is the distribution at L_w, bimodal but it is also skewed slightly towards lower energies. By 2.5 L_w the distribution has reacquired a nearly Gaussian form, with a width similar to that at 0.015 L_w.

The pattern that the energy fluctuations initially increase, peak, and then decrease is repeated throughout all the simulations to be presented. It is therefore worthwhile to explain this overall behavior here. A good analogy for understanding this cycle is to envision the total Stokes energy, as the

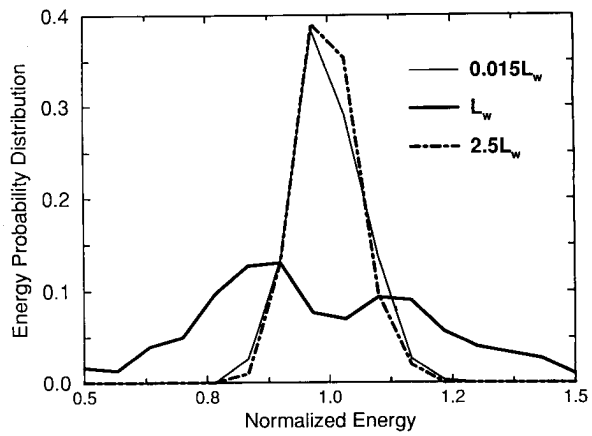

Fig. 5. Stokes-pulse energy probability distributions versus energy normalized to the average energy of a given ensemble at fiber lengths of 0.015 L_w, L_w and 2.5 L_w, under the same conditions as Fig. 1.

cumulative sum of the energy of all the Stokes photons of various frequencies. The energy values of the photons that can be amplified, and the probability of a photon of a particular energy being amplified, can be determined from the frequency distribution of the Raman gain spectrum. The ratio of the widths of the Raman-gain spectrum to the pump-pulse spectrum determines the number of different frequency components that can contribute to the Stokes pulse growth. In (28) this ratio is approximated by ΓT_p. Initially, only the frequency components at the peak of the Raman-gain spectrum are above threshold and are amplified. The energy fluctuations are relatively low, as seen at $z = 0.015\ L_w$. As the pulses propagate in the fiber, more frequency components satisfy the threshold condition given by (25). This factor corresponds to the denominator of (28). The range of frequencies amplified widens, increasing the energy fluctuations of the Stokes pulse. This agrees with the results in Fig. 5 at $z = L_w$. Eventually, the fluctuations decrease because the frequency components that are initially highly amplified saturate the pump, while those components that received less amplification continue to grow. In the limit of total pump depletion, all the energy of the pump pulse is transferred to the Stokes pulse, and the energy fluctuations stabilize. In Fig. 5 at $z = 2.5\ L_w$, the fluctuations decrease as the tail of Stokes pulse begins to deplete the pump pulse.

This pattern is predicted from the work on gases. The parameters m is calculated to be 139 at $z = 0.015\ L_w$, which clearly predicts Gaussian statistics. At $z = L_w$, the value of this parameter has fallen and is now $m = 2$, which indicates the energy distribution will have less of a Gaussian shape. Finally, at $z = 2.5\ L_w$ the nonlinear regime has been reached and there is some pump depletion. This reduces energy fluctuations and suggests once again nearly Gaussian statistics [18].

With this overall pattern established, Fig. 6 is a plot of the normalized standard deviation of the Stokes pulse energy distributions under various conditions. Curve (i) is a plot for the conditions described in Fig. 1, curve (ii) is with zero SPM, XPM, GVD and walk-off, and curve (iii) was obtained using the same parameters as in Fig. 1 except the input pump

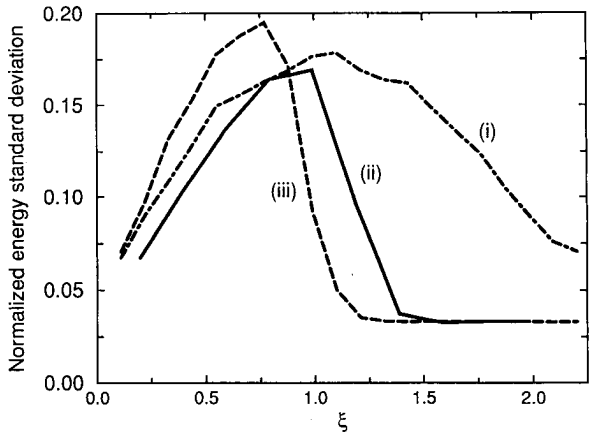

Fig. 6. Stokes pulse energy standard deviation normalized to average Stokes energy versus fiber length normalized to walk-off length for values of (i) same parameters as Fig. 1, (ii) same as Fig. 1 with $\gamma_p = \gamma_s = \beta_{2p} = \beta_{2s} = d = 0$ and (iii) same as Fig. 1 with $P_0 = 1.5P_{\text{th}}$.

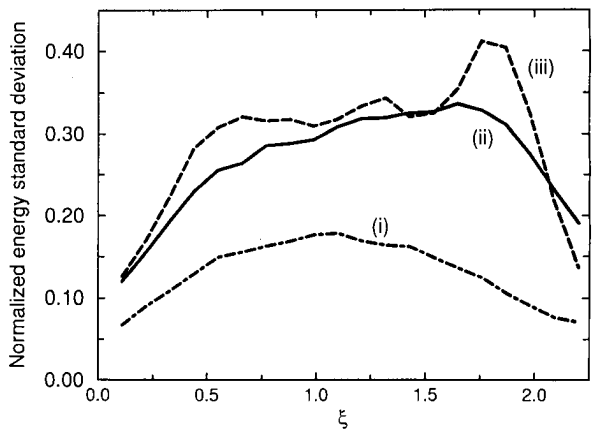

Fig. 7. Stokes pulse energy standard deviation normalized to average Stokes energy versus fiber length normalized to walk-off length with (i) same parameters as Fig. 1, (ii) same as Fig. 1 with $T_p = 2$ ps $\gamma_p = \gamma_s = \beta_{2p} = \beta_{2s} = d = 0$, and (iii) same as Fig. 1 with $T_p = 2$ ps and $\beta_{2p} = \beta_{2s} = 0$.

power is now $P_0 = 1.5P_{\text{th}}$. The behavior seen in curve (i) was described above using Fig. 5 and is shown here for reference. Curve (ii) shows that the energy fluctuations without nonlinear or dispersive effects initially follows the behavior of curve (i), but the energy fluctuations are dampened after a much shorter length of fiber. This is because for the parameters of curve (ii), the Stokes pulse does not walk away from the pump pulse, and the pump pulse does not broaden temporally or spectrally. Depletion of the pump pulse occurs over much shorter lengths of fiber, and therefore so to does the corresponding stabilization of energy statistics. A result which agrees with the work on gases.

Curve (iii) shows that the the effect of increasing pump power is to initially increase energy fluctuations, but at the same time to cause them to decrease after a shorter length of fiber. Returning to the analogy being used, a higher input pump power means that a larger number of frequency components satisfy the power threshold condition and are amplified, which increases energy fluctuations. However, stabilization of energy statistics occurs for shorter lengths of fiber due to the more rapid depletion of the pump. This behavior is also predicted by (28). A higher input power reduces the value of m.

Fig. 7 shows the standard deviation of energy distributions versus normalized distance under three different conditions. Curve (i) is for the same parameters as curve (i) in Fig. 6 and is shown here for reference. Curves (ii) and (iii) are for 2 ps pulses, with an input pump power 20% above threshold with (ii) GVD 0 and (iii) GVD $\neq$ 0. Fig. 7 shows that energy fluctuations increase when the pump-pulse width is reduced. For a narrower pulse width, the frequency spectrum of the pump pulse is broader, which in our analogy means more frequency components are amplified, and hence energy fluctuations are increased. Reducing the input pump-pulse width reduces m, which also predicts increased fluctuations in the Stokes pulse energy. Again, the work here corresponds to that done for gases.

The differences in curves (ii) and (iii) of Fig. 7 suggests that the effect of GVD is to reduce the variations in Stokes energy. When GVD is present, the pump pulse spreads and its peak intensity decreases. This means that the number of frequency components above threshold decreases, leading to reduced energy fluctuations. There is a kink in the energy fluctuations when there is no GVD (curve (iii)). This kink corresponds to the amplification of a secondary Stokes pulse after the initial Stokes pulse has walked off from the pump pulse. As the Stokes pulse begins to deplete the pump pulse, there is a rapid drop in the energy fluctuations, and shortly after $2L_w$ the standard deviation for the case of zero GVD has dropped below that of the situation where GVD is present. In gases it was noted that an increase in diffraction increased energy fluctuations by preventing depletion of the pump pulse [18]. In Fig. 7 this result is seen by the fact that the energy fluctuations without GVD begin to dip below that with GVD before a secondary Stokes pulse is amplified.

B. Pulse Width

The behavior of the temporal fluctuations follows the same trend as the energy fluctuations with few exceptions. Specifically, temporal fluctuations also initially increase as the pulses propagate down the fiber, then peak and eventually start to decline. In some sense this pattern is expected. As energy is being added to the Stokes pulse its width will also be changing. As the energy fluctuate so too should its width.

One noticeable difference between the width distribution and energy fluctuations is the rate at which fluctuations decrease. Fig. 8 shows the temporal fluctuations at $z = 2.5\ L_w$ have not reduced to a width comparable to that at $z = 0.015\ L_w$ as is the case for energy shown in Fig. 5. This is because energy fluctuations are stabilizing through the growth of the tail in the Stokes pulse. If the Stokes pulse has significantly (slightly) depleted the pump pulse, the tail of the Stokes pulse is weakly (strongly) amplified. In these two extremes, the energy transferred to the Stokes pulse is about equal, but the pulse widths are very different.

The pulse width fluctuations corresponding to the energy fluctuations in Fig. 6 are not shown here since they have

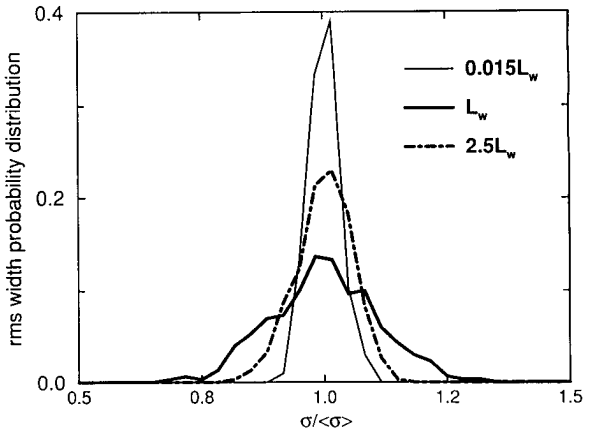

Fig. 8. Stokes pulse-width probability distributions versus rms pulse width normalized to the average rms width at fiber lengths of 0.015 L_w, L_w, and 2.5 L_w, under the same conditions as Fig. 1.

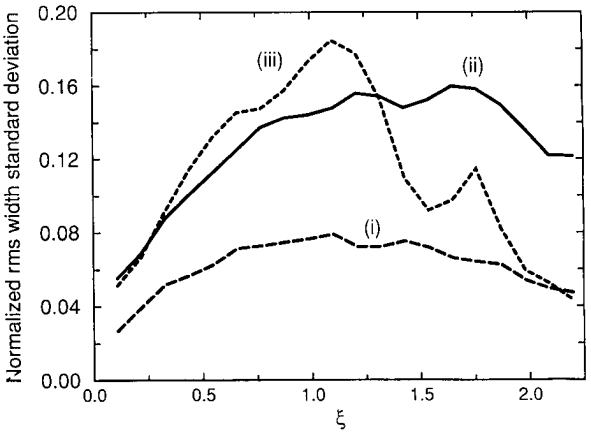

Fig. 9. Stokes pulse width standard deviation normalized to average Stokes pulse width versus fiber length normalized to walk-off length with parameters corresponding to those in Fig. 7 for the various curves.

the same qualitative behavior as the energy fluctuations. The most striking difference between the temporal fluctuations and energy fluctuations can be seen by comparing Fig. 7 with 9. Fig. 9 shows the pulse width fluctuations under the same conditions as in Fig. 7. The major difference seen here is that GVD affects temporal fluctuations much more than it does energy fluctuations. When there is no GVD, the Stokes pulse walks away from the pump pulse after a shorter length of fiber, and the pump pulse begins to amplify the tail of the Stokes pulse. Therefore even though there are large fluctuations in the energy, the width of the Stokes pulse is steadily broadening with less fluctuations. Again a kink corresponding to the amplification of a secondary Stokes pulse is observed.

VIII. Conclusion

In this paper, a model for the build up of the Stokes pulse during stimulated Raman scattering of picosecond pulses has been presented. A Langevin-noise term and an experimentally obtained Raman-gain spectrum were used in coupled nonlinear Schrödinger equations. The results show that the temporal profile of the Stokes pulse initially narrows during growth and then expands, whereas the spectrum narrows and remains fairly constant. The effect of GVD was seen to be negligible on both Stokes energy transfer and compression for pulse widths as narrow as 10 ps. The effect of lowering the pump pulse width to 2 ps was to reduce the amount of energy transferred and the pulse narrowing of the Stokes pulse. The GVD effects become important for 2-ps pump pulses. Increasing the pump power increases Stokes-pulse amplification while reducing the minimum pulse width.

The shot-to-shot fluctuations of the Stokes-pulse energy and temporal width were also examined. It was seen that the energy and pulse width fluctuations both initially increase with fiber length, then decrease in the regime of pump depletion. This behavior was observed under a variety of pump pulse and fiber conditions. The effect of reducing pump pulse width was to increase both energy and pulse fluctuations of the Stokes pulse. An increase in the input pump power, while causing an initial increase in the Stokes energy and pulse width fluctuations, also causes a decrease in the length of fiber needed before fluctuations are damped. The presence of GVD reduces Stokes fluctuations, but by dispersing the pump pulse, it delays the onset of pump depletion and the corresponding reduction in fluctuations. However, the effect of GVD is more significant for fluctuation in pulse widths than energy.

Acknowledgment

Thanks and appreciation are expressed to R. H. Stolen for supplying the Raman gain spectrum. It is a pleasure to acknowledge helpful discussions with I. A. Walmsley and J. W. Haus.

References

[1] G. P. Agrawal, *Nonlinear Fiber Optics.* San Diego, CA: Academic, 1989.
[2] E. J. Woodbury and W. K. Ng, "Ruby laser operation in the near IR," *Proc. IRE,* vol. 50, p. 2367, 1962.
[3] R. H. Stolen, E. P. Ippen, and A. R. Tynes, "Raman oscillation in glass optical waveguide," *Appl. Phys. Lett.,* vol. 20, pp. 62–64, 1972.
[4] R. H. Stolen and E. P. Ippen, "Raman gain in glass optical waveguides," *Appl. Phys. Lett.,* vol. 22, pp. 276–278, 1973.
[5] G. P. Agrawal, *Nonlinear Fiber Optics.* San Diego, CA: Academic, 1989, ch. 8.
[6] P. N. Kean, K. Smith, and W. Sibbet, "Spectral and temporal investigation of self-phase modulation and stimulated Raman scattering in a single-mode optical fibre," *IEE Proc.,* vol. 134, pt. J, pp. 163–170, 1987.
[7] C. Headley, III, and G. P. Agrawal, "Simultaneous amplification and compression of picosecond optical pulses during Raman amplification in optical fibers," *J. Opt. Soc. Am. B,* vol. 10, pp. 2383–2389, 1993.
[8] J. P. Gordon, "Theory of the soliton self-frequency shift," *Opt. Lett.,* vol. 11, pp. 662–664, 1986.
[9] F. M. Mitsche and L. F. Mollenauer, "Discovery of the soliton self-frequency shift," *Opt. Lett.,* vol. 11, pp. 659–661, 1986.
[10] G. P. Agrawal, *Nonlinear Fiber Optics.* San Diego, CA: Academic, 1989, ch. 4.
[11] ——, *Nonlinear Fiber Optics.* San Diego, CA: Academic, 1989, ch. 7.
[12] R. H. Stolen, C. Lee, and R. K. Jain, "Development of the stimulated Raman spectrum in single-mode silica fibers," *J. Opt. Soc. Am. B.,* vol. 1, pp. 652–657, 1984.
[13] K. X. Liu and E. Garmire, "Understanding the formation of the SRS Stokes spectrum in fused silica fibers," *IEEE J. Quantum Electron.,* vol. 27, pp. 1022–1030, 1991.

[14] V. A. Aleshkevich, G. D. Kozhoride, and M. V. Shamonin, "Generation of Stokes stimulated Raman scattering pulses from spontaneous noise in fiber lightguides," *J. Commun. Tech. and Elec.,* vol. 38, pp. 104–109, 1993.
[15] For a recent review see M. C. Raymer and I. A. Walmsley, "The quantum coherence properties of stimulated Raman scattering," in *Progress in Optics,* E. Wolf, Ed. Amsterdam: North Holland/Elsevier, 1990.
[16] M. G. Raymer, I. A. Walmsley, J. Mostowski, and B. Sobolewska, "Quantum theory of spatial and temporal coherence properties of stimulated Raman scattering," *Phys. Rev. A,* vol. 32, pp. 332–344, 1985.
[17] I. A. Walmsley and M. G. Raymer, "Experimental study of the macroscopic quantum fluctuations of partially coherent stimulated Raman scattering," *Phys. Rev. A,* vol. 33, pp. 382–390, 1986.
[18] I. A. Walmsley, M. G. Raymer, T. Sizer, II, I. N. Duling, III, and J. D. Kafka, "Stabilization of Stokes pulse energies in the nonlinear regime of stimulated Raman scattering," *Opt. Commun.,* vol. 53, pp. 137–140, 1985.
[19] M. Scalora and J. W. Haus, "Quantum fluctuations and diffraction in stimulated Raman scattering," *Opt. Commun.,* vol. 87, pp. 267–272, 1992.
[20] C. S. Wang, "Theory of stimulated Raman scattering," *Phys. Rev.,* vol. 182, pp. 482–494, 1969.
[21] R. H. Stolen, private communication.
[22] R. H. Stolen, J. P. Gordon, W. J. Tomlinson, and H. A. Haus, "Raman response function of silica-core fibers," *J. Opt. Soc. Am. B,* vol. 6, pp. 1159–1166, 1989.
[23] K. J. Blow and D. Wood, "Theoretical description of transient stimulated Raman scattering in optical fibers," *IEEE J. Quantum. Electron.,* vol. 25, pp. 2665–2673, 1989.
[24] A. Höök, "Influence of stimulated Raman scattering on cross-phase modulation between waves in optical fibers," *Opt. Lett.,* vol. 17, pp. 115–117, 1992.
[25] F. X. Kärtner, D. J. Dougherty, H. A. Haus, and E. P. Ippen, "Raman noise and soliton squeezing," *J. Opt. Soc. Am. B,* vol. 11, pp. 1267–1276, 1994.
[26] R. W. Boyd, *Nonlinear Optics.* San Diego, CA: Academic, 1992.
[27] C. Headley, "Ultrafast stimulated Raman scattering in optical fibers," Ph.D. thesis, Inst. of Optics, Univ. of Rochester, Rochester, NY, 1995.
[28] R. W. Boyd, *Radiation and Detectors.* New York: Wiley, 1983.
[29] W. H. Press, B. P. Flannery, S. A. Teukolsky, and W. T. Vetterling, *Numerical Recipes.* New York: Cambridge Univ. Press, 1986.

Clifford Headley, III was born December 13, 1964, and raised in Nassau, Bahamas. He received the B.S. and M.S. degrees in electrical engineering from the University of Texas, Arlington, TX, in 1986 and 1988, respectively, and the Ph.D. degree in optics from the University of Rochester's Institute of Optics, NY, in 1995. His M.S. research was in measuring the electron density of a plasma arc, and his Ph.D. research was concerned with nonlinear effects in fiber optics and ultrafast pulse propagation.

He is currently at AT&T Bell Labs, where his research interests are nonlinear effects in fiber optics and high-power amplifiers and lasers.

Govind P. Agrawal (M'83–SM'86) received the B.S. degree from the University of Lucknow, India, in 1969, and the M.S. and Ph.D. degrees from the Indian Institute of Technology, New Delhi, in 1971 and 1974, respectively.

After holding positions at the École Polytechnique, France, the City University of New York, NYC, and AT&T Bell Laboratories, Murray Hill, NJ, Dr. Agrawal joined the faculty of the Institute of Optics at the University of Rochester, in 1989, where he is a professor of optics. His research interests focus on quantum electonics, nonlinear optics, and laser physics. In particular, he has contributed significantly to the fields of semiconductor lasers, nonlinear fiber optics, and optical communications.

Dr. Agrawal is a Fellow of the Optical Society of America. He is an author and coauthor of more than 200 research papers, several book chapters and review articles, and three books: *Semiconductor Lasers*, Van Nostrand Reinhold, 1993, *Nonlinear Fiber-Optic Communication Systems*, Wiley, 1992. He has also edited several books.